Available online at www.sciencedirect.com
ScienceDirect
Journal of the European Ceramic Society 30 (2010) 2593–2601
www.elsevier.com/locate/jeurceramsoc

Effect of oxide additives on the sintering behavior and electrical properties of strontium- and magnesium-doped lanthanum gallate

Sang Bu Ha [a], Yoon Ho Cho [a], Yun Chan Kang [b], Jong-Ho Lee [c], Jong-Heun Lee [a,*]

[a] *Department of Materials Science and Engineering, Korea University, 1, 5-ka, Anam-dong, Sungbuk-ku, Seoul 136-713, South Korea*
[b] *Department of Chemical Engineering, Konkuk University, Seoul 143-701, South Korea*
[c] *Center for Energy Materials Research, Korea Institute of Science and Technology, Seoul 136-791, South Korea*

Received 23 February 2010; accepted 12 May 2010
Available online 9 June 2010

Abstract

The effects of 14 different metal-oxide additives (metal = Mn, Fe, Co, Ni, Cu, B, Li, V, Zn, Si, Ca, Al, Bi, and Ba) on the sintering, phase purity, and electrical properties of strontium- and magnesium-doped lanthanum gallate (LSGM) are studied. The density, phase purity, and electrical conductivity depend closely on the sintering aids and sintering temperatures. The addition of V, Zn, Si, Co, and Fe improves the densification, phase purity, and electrical conductivity, with V showing the most promising effect on the low-temperature sintering of the phase-pure LSGM specimen with high conductivity.

Keywords: Strontium- and magnesium-doped lanthanum gallate; Fuel cell; Sintering; Ionic conductivity; Impedance

1. Introduction

Strontium- and magnesium-doped lanthanum gallate (LSGM) is one of the representative electrolytes for application to solid oxide fuel cells (SOFCs).[1,2] Its high ionic conductivity and stability over a wide range of oxygen partial pressures ($Po_2 = 10^{-22}$–1 atm) support SOFC operation at an intermediate temperature regime (~700 °C). The operation temperature can be decreased further by thinning the electrolyte layer using anode-supported design.[3–6]

Generally, the densification of LSGM up to a gas-impermeable level requires a very high sintering temperature (~1500 °C).[7] Due to the complex cation composition, a number of intermediate phases are known to form when sintered or calcined at low temperatures.[8–10] Moreover, high-temperature sintering often leads to the formation of a highly resistive interface phase between the electrolyte and anode.[11] Thus, various oxide buffer layers such as La_2O_3-doped ceria,[12] Gd_2O_3-doped ceria (GDC),[13] Sm_2O_3-doped ceria[14,15] and scandia-stabilized zirconia[13] have been employed to block the interdiffusion of La and Ni components from the electrolyte and anode layers.

Accordingly, the densification of phase-pure LSGM at low sintering temperature is a very important and challenging hurdle that must be overcome in order to accomplish the following three objectives: (1) low temperature fabrication of SOFCs, (2) fabrication of a highly conductive solid electrolyte, and (3) the prevention of interface reaction during sintering. The sintering temperature of LSGM can be decreased either by adopting new processing techniques or by employing sintering additives. Recent processing efforts can be divided into two categories: the preparation of well-sinterable powders and the use of innovative consolidation techniques. The former includes carbonate coprecipitation,[16,17] citrate method,[9] glycine nitrate method,[18,19] organic precursor method,[20] hydrothermal urea precipitation,[21] spray pyrolysis,[22] mechanochemical synthesis[23] and self-propagating high-temperature synthesis.[24] The latter process category includes spark plasma sintering,[25,26] atmosphere-controlled sintering,[27] microwave sintering[28,29] and hot isostatic pressing.[30] The above research illustrates the great importance of the low-temperature sintering of LSGM.

Various sintering additives can also be used to enhance the densification, although they sometimes deteriorate the purity or ionic conductivity of the electrolyte. The oxides of various

* Corresponding author. Tel.: +82 2 3290 3282; fax: +82 2 928 3584.
E-mail addresses: jongheun@korea.ac.kr, leejongheun@gmail.com (J.-H. Lee).

0955-2219/$ – see front matter © 2010 Elsevier Ltd. All rights reserved.
doi:10.1016/j.jeurceramsoc.2010.05.007

transition metals such as Co,[31–36] Fe,[31,32,35,37,38] Mn,[31,32] Ni,[31] Cu,[31] and Cr[32] have been explored to improve the ionic conductivity of LSGM by the b-site control of perovskite materials. Among these, Fe and Co enhance the ionic conductivity significantly with a slight decrease of ionic transport number.[31–36] In another positive contribution toward the use of sintering additives, the phase stability of LSGM[39] and the power density of SOFCs[38] were improved by the addition of Fe. This demonstrates that the proper design of sintering additives for LSGM can significantly enhance the performance of LSGM-based SOFCs by improving the density, ionic conductivity, phase stability, and interface stability of the electrolyte.

In the present study, 14 different sintering additives were added to LSGM electrolytes and their effects on the sintering behavior, electrical conductivity, and phase purity were systematically investigated. The main focus was directed at finding new and effective sintering additives to be capable of lowering the sintering temperature, decreasing the secondary phase, and enhancing the ionic conductivity.

2. Experimental

The LSGM ($La_{0.8}Sr_{0.2}Ga_{0.8}Mg_{0.2}O_{2.8}$) powders were prepared by the glycine nitrate method. $La(NO_3)_3{\cdot}6H_2O$ (99.99%, Aldrich, USA), $Sr(NO_3)_2$ (>99%, Sigma–Aldrich, USA), $Ga(NO_3)_3{\cdot}xH_2O$ (99.9%, Aldrich, USA) and $Mg(NO_3)_2{\cdot}6H_2O$ (99%, Sigma–Aldrich, USA) were dissolved in 150 mL of distilled water ($[La^{3+}]:[Sr^{2+}]:[Ga^{3+}]:[Mg^{2+}] = 8:2:8:2$), to which H_2NCH_2COOH (glycine, >99%, Sigma, USA) was added ($[\text{glycine}]/([La^{3+}] + [Sr^{2+}] + [Ga^{3+}] + [Mg^{2+}]) = 1.0$). The polymeric gel precursor was prepared by heating the stock solution at 80 °C for 10 h. The LSGM powders were prepared by calcining the precursors at 1000 °C for 2 h.

The 1 at% of the sintering aids was added by ball milling a mixture of LSGM powders and the additives in the forms of oxides or the salts containing corresponding cations in C_2H_5OH for 24 h. The source materials were $Mn(NO_3)_2{\cdot}4H_2O$ (>97%, Sigma, USA), $Fe(NO_3)_3{\cdot}9H_2O$ (>98%, Aldrich, USA), $Co(NO_3)_2{\cdot}6H_2O$ (>97%, Junsei Chemical, Japan), $Ni(NO_3)_2{\cdot}6H_2O$ (>97%, Aldrich, USA), $Cu(NO_3)_2{\cdot}3H_2O$ (>99.5%, Junsei Chemical, Japan), SiO_2 sol (ST-0, solvent water, 20.4 wt.% SiO_2, Nissan Chemical, Japan), B_2O_3 (>99.99%, High Purity Chemicals, Japan), V_2O_5 (>99%, Junsei Chemical, Japan), $Zn(NO_3)_2{\cdot}6H_2O$ (99%, Kanto Chemical Co., Japan), $Li(C_2H_3O_2)$ (99.99%, Aldrich, USA), $Bi(NO_3)_3{\cdot}5H_2O$ (>98%, Sigma–Aldrich, USA), $Al(NO_3)_3{\cdot}9H_2O$ (>98%, Sigma–Aldrich, USA), $Ba(C_2H_3O_2)_2$ (99%, Sigma–Aldrich, USA), and $Ca(NO_3)_2{\cdot}4H_2O$ (>98.5%, Kanto Chemical Co., Japan). After drying and pulverization, the specimens were isostatically pressed at 150 MPa and sintered in air at 1200 and 1300 °C for 4 h. For simplicity, the specimens doped with sintering aids are referred to as 'LSGM-M-ST' where

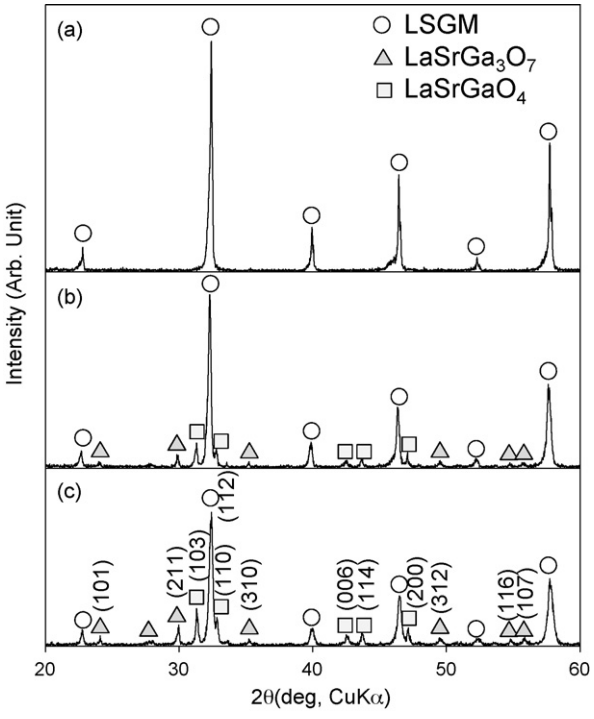

Fig. 1. X-ray diffraction (XRD) patterns of LSGM powders sintered at (a) 1400, (b) 1300, and (c) 1200 °C.

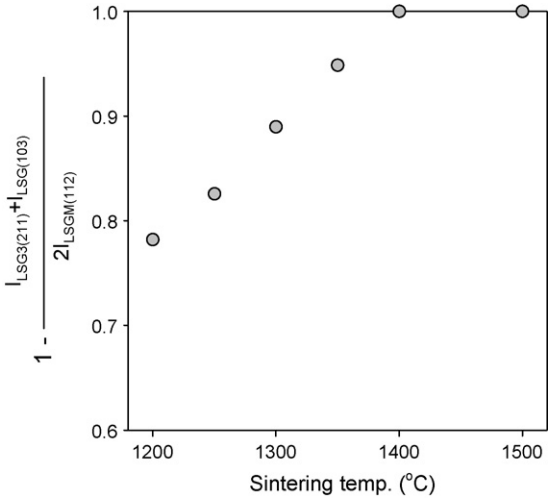

Fig. 2. Phase purity of LSGM as a function of sintering temperature. $I_{LSG3(211)}$, $I_{LSG(103)}$ and $I_{LSGM(112)}$ are the intensities of the (2 1 1) peak of $LaSrGa_3O_7$, (1 0 3) peak of $LaSrGaO_4$ and (1 1 2) peak of LSGM, respectively.

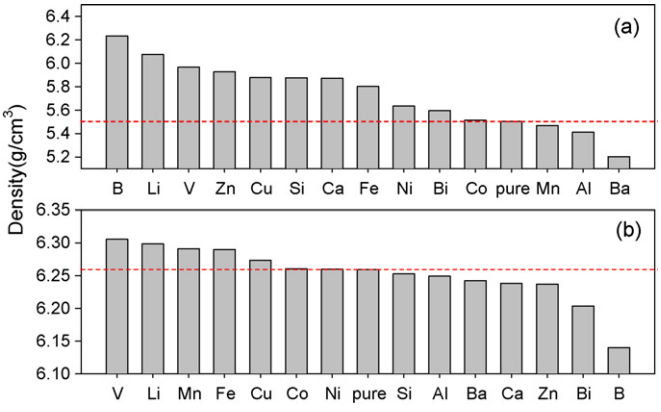

Fig. 3. Apparent densities of specimens sintered at (a) 1200 °C and (b) 1300 °C.

'M' and 'ST' are the metal component of the additive and the sintering temperature, respectively. For example, LSGM-Si-1200 indicates the SiO_2-doped LSGM specimens sintered at 1200 °C.

The apparent density of the sintered body was measured using the Archimedes method in deionized water. The phases of the sintered specimens were analyzed by X-ray diffraction (XRD, Rmax/c, Rigaku Co., Tokyo, Japan). After applying a Pt electrode using Pt paste (TR7905, Tanaka Co., Tokyo, Japan), the complex impedance was measured at 300 °C in air using an impedance analyzer (Alpha-N, Novocontrol Tech., Germany).

3. Results and discussion

3.1. X-ray diffraction (XRD)

After the calcination of the precursors at 1000 °C, the LSGM powders contained the second phases such as $LaSrGa_3O_7$ (LSG3) and $LaSrGaO_4$ (LSG) (not shown). The amount of second phase decreased with increasing sintering temperature (Fig. 1). At a sintering temperature of 1400 °C, pure LSGM phase was prepared. As a measure of the LSGM phase purity, the *PP* factor was employed using the intensity of peaks for

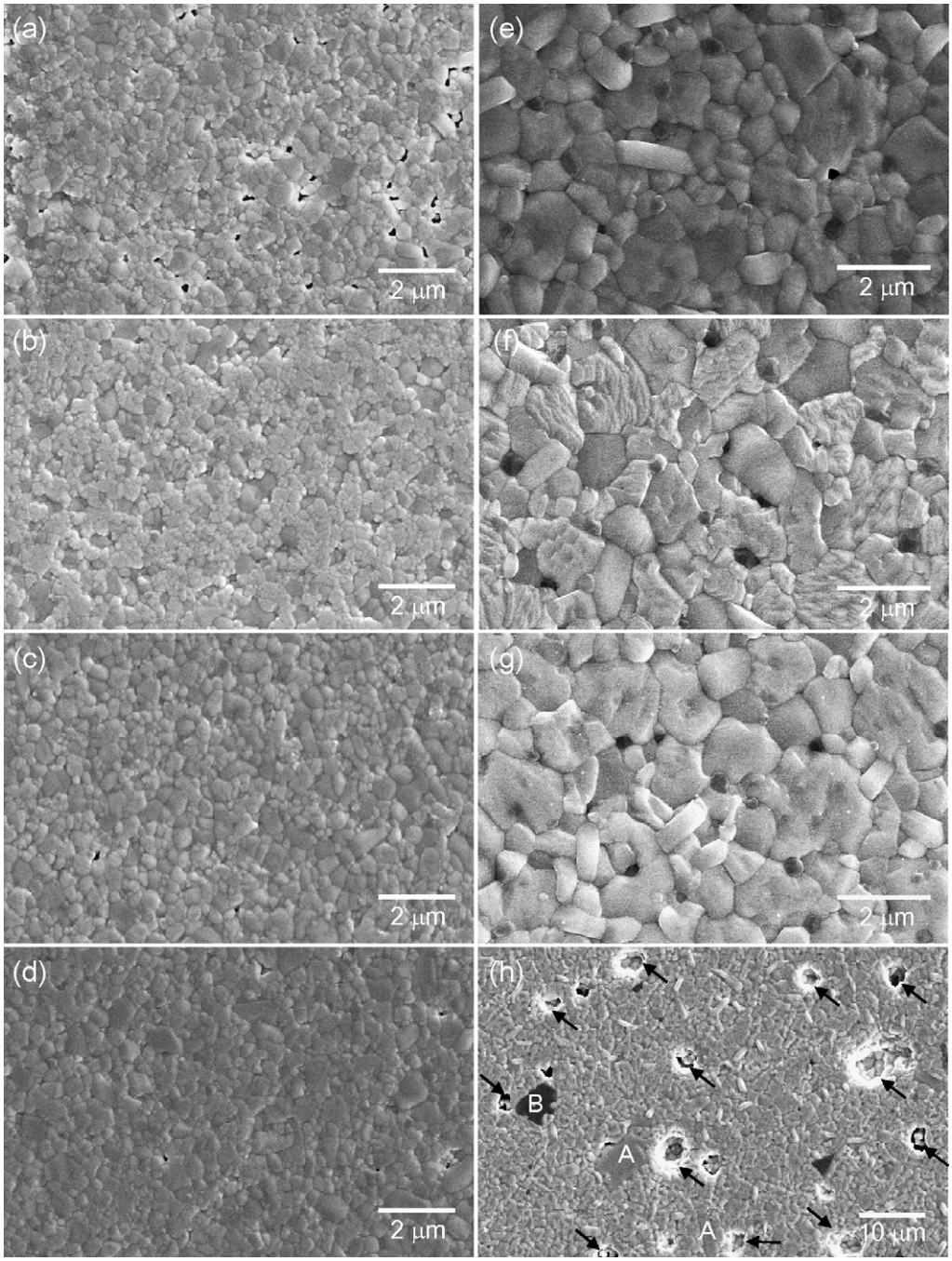

Fig. 4. SEM images of (a) LSGM-1200, (b) LSGM-V-1200, (c) LSGM-Zn-1200, (d) LSGM-B-1200, (e) LSGM-1300, (f) LSGM-V-1300, (g) LSGM-Zn-1300 and (h) LSGM-B-1300 specimens.

LSG3 and LSG phases relative to that for the LSGM phase, as in Eq. (1):

$$PP = 1 - \frac{I_{\mathrm{LSG3(211)}} + I_{\mathrm{LSG(103)}}}{2I_{\mathrm{LSGM(112)}}} \quad (1)$$

where $I_{\mathrm{LSG3(211)}}$, $I_{\mathrm{LSG(103)}}$ and $I_{\mathrm{LSGM(112)}}$ are the intensities of the (2 1 1) peak of $LaSrGa_3O_7$, the (1 0 3) peak of $LaSrGaO_4$ and the (1 1 2) peak of LSGM, respectively. The *PP* factor is defined such that it is higher for the purer LSGM phase and tends to unity for the completely pure specimen. The *PP* factor was increased from 0.78 to 1 as the sintering temperature was increased from 1200 to 1400 °C (Fig. 2).

3.2. Densification and phase purity

The apparent densities of the specimens doped with various sintering additives are shown in Fig. 3. For convenience, the specimens were sorted according to their densities. Except Mn, Al, and Ba, all the sintering aids increased the density at a sintering temperature of 1200 °C (Fig. 3(a)), while the densification was promoted by doping with V, Li, Mn, Fe, Cu, Co, and Ni when sintered at 1300 °C (Fig. 3(b)). Fig. 4 shows the SEM images of LSGM, LSGM-V, LSGM-Zn and LSGM-B specimens sintered at 1200 and 1300 °C. At the sintering temperature of 1200 °C, the porosity was greatly decreased by doping with V, Zn and B (Fig. 4(a)–(d)). As increasing sintering temperature to 1300 °C, the grains were coarsened (Fig. 4(e)–(h)). Note that a few very large grains were found in LSGM-B-1300 specimen (A and B in Fig. 4(h)). This indicates the abnormal grain growth. Although the theoretical densities of the specimens differ according to the kinds of additive, the theoretical density could not be calculated due to the lack of information on the incorporation of dopants into the LSGM lattice. Nevertheless, the increase or decrease of density in Fig. 3 can be used as a measure of densification due to the very low concentration of sintering aids (1 at%).

The effects of sintering additives on the phase purity of LSGM differed; the results are summarized in Fig. 5 and the representative XRD patterns are shown in Fig. 6. The relative intensities of the second phases were closely dependent on the sintering aids. At a sintering temperature of 1200 °C, the phase purity was increased by doping with V, B, Fe, Si, Al, Zn, Ni, and Cu (Fig. 5(a)). On the other hand, most of sintering additives,

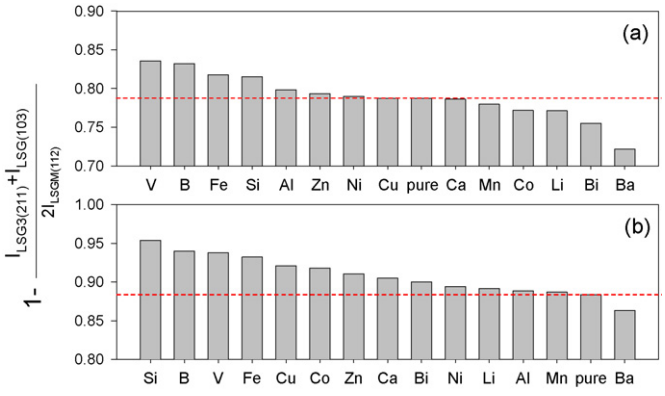

Fig. 5. Phase purity of the specimens sintered at (a) 1200 °C and (b) 1300 °C.

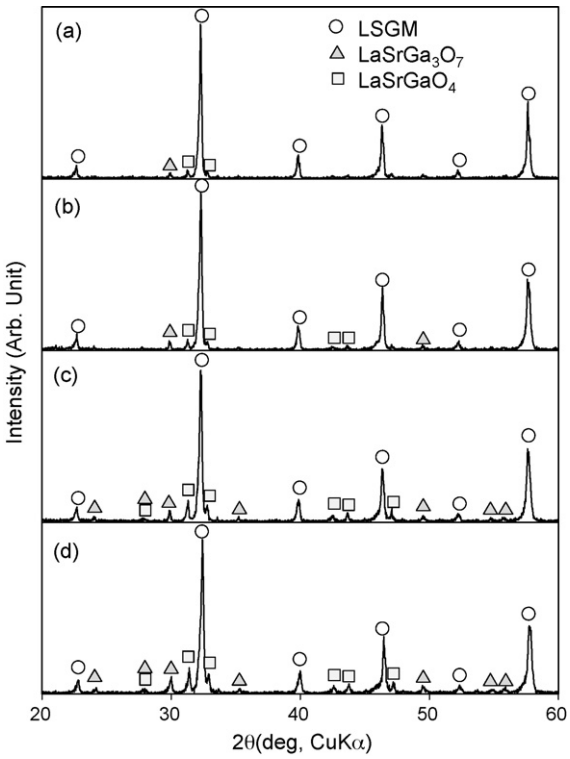

Fig. 6. X-ray diffraction (XRD) patterns of (a) LSGM-Si-1300, (b) LSGM-V-1300, (c) LSGM-1300, and (d) LSGM-Ba-1300 specimens.

except Ba, increased the phase purity when sintered at 1300 °C (Figs. 5(b) and 6).

3.3. Complex impedance analysis

Complex impedances were measured at 300 °C and the representative results are shown in Fig. 7. The three contributions from the low frequency range are those from electrode polarization, grain boundary, and grain interior, respectively. From the impedance spectra, grain-interior resistivity (ρ_{gi}) and apparent grain-boundary resistivity ($\rho_{gb}{}^{app}$) were attained. Fig. 8 summarizes the results for the specimens sintered at 1200 and 1300 °C. The $\rho_{gb}{}^{app}$ values of all the specimens were greatly decreased when the sintering temperature was increased from 1200 to 1300 °C while the changes of ρ_{gi} values were relatively small (Fig. 8(a) and (b)). The $\rho_{gb}{}^{app}$ value depends on the grain-boundary density, that is, the grain size, because it is calculated simply from the electrode area (A) and the specimen thickness (l). Thus, the smaller $\rho_{gb}{}^{app}$ values at the higher sintering temperature can be attributed to the effect of grain growth (see SEM images in Fig. 4) in decreasing the grain-boundary density.

When sintered at 1200 °C, the total resistivity ($\rho_{tot} = \rho_{gi} + \rho_{gb}{}^{app}$) was increased by the addition of Bi, Ni, and Ba, but decreased by the addition of other sintering aids (Fig. 8(a)). At a sintering temperature of 1300 °C, most of the sintering aids except Bi, Ba, and B enhanced the total conductivity (Fig. 8(b)). A careful examination of Figs. 7 and 8 reveals that the ρ_{gi} values were also influenced by the addition of sintering aids. This can be explained in part by the incorporation of sintering aids into the LSGM lattice and its consequent effect

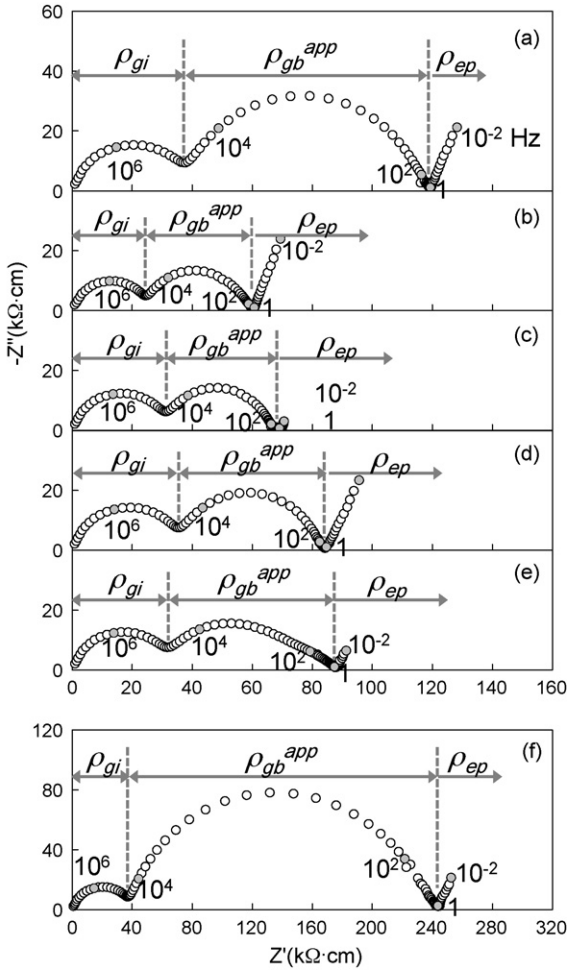

Fig. 7. Complex impedance spectra of (a) LSGM-1300, (b) LSGM-V-1300, (c) LSGM-Fe-1300, (d) LSGM-Zn-1300, (e) LSGM-Co-1300, and (f) LSGM-Bi-1300 specimens at 300 °C in air.

on the grain-interior conduction. However, the slight change of ρ_{gi} values due to the variation of effective cross-sectional area for conduction via densification should also be taken into account.

3.4. The effect of B

The addition of B greatly increased the phase purity of LSGM regardless of the sintering temperature (Fig. 5). However, B addition induced a wide divergence in densification behavior according to the sintering temperature. The B-doped specimen showed the highest density at 1200 °C (Fig. 3(a)), but the lowest at 1300 °C (Fig. 3(b)). The addition of B_2O_3 has been reported to promote densification by liquid phase sintering mechanism[40–43] and lower the phase formation temperature by the acceleration of mass transfer via the liquid phase.[41,42] The dense microstructure in Fig. 4(d) can be understood in this viewpoint. Densification, however, can be hindered by the evaporation of B_2O_3 when the sintering temperature becomes higher than 1100–1300 °C.[41–43] The temperatures for the evaporation of B_2O_3 were dependent upon the formation of different binary and ternary eutectic compositions by interacting with different host oxide materials.

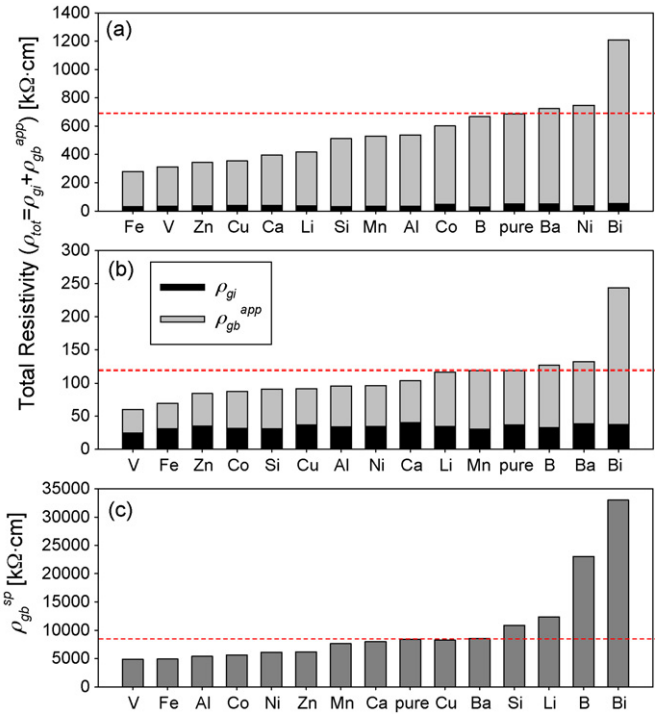

Fig. 8. Total resistivity ($\rho_{tot} = \rho_{gi} + \rho_{gb}^{app}$) of specimens sintered (a) 1200 °C and (b) 1300 °C, and (c) specific grain-boundary resistivity (ρ_{gb}^{sp}) of specimens sintered at 1300 °C.

Many large pores found at LSGM-B-1300 specimen (arrows in Fig. 4(h)) were attributed to the evaporation of B_2O_3. Above explains the increase of phase purity and density at 1200 °C and the low density at 1300 °C. The ρ_{tot} values of the LSGM-B specimens were similar to those of the LSGM specimens (Fig. 8). These results indicate that the addition of B has the potential to accomplish the low-temperature sintering of phase-pure LSGM but is not desirable for the densification at high temperatures.

3.5. The effect of Zn

The addition of Zn increased the density at a sintering temperature of 1200 °C (Fig. 3(a)). However, the density of LSGM-Zn-1300 was slightly lower than that of LSGM-1300 (Fig. 3(b)). The promotion of sintering by the addition of ZnO is relatively well known in dielectric materials,[44–46] piezoelectric materials[47] and solid oxide proton conductors,[48–50] although the mechanism for the enhanced sintering differs according to the material systems. Moreover, like B_2O_3, ZnO is known to evaporate at ~1300 °C.[51] Accordingly, the promotion and slight deterioration of sintering in comparison to the undoped LSGM specimens at 1200 and 1300 °C can be explained by the ZnO-assisted sintering and the evaporation of ZnO, respectively. The *PP* factors were increased slightly by the addition of Zn (Fig. 5). The effect of Zn on the electrical conductivity was more significant. The ρ_{tot} values of LSGM-Zn-1200 and LSGM-Zn-1300 were 345.0 and 84.3 kΩ cm, respectively (Fig. 8), which were substantially smaller than those of LSGM-1200 and LSGM-1300 (686.5 and 119.2 kΩ cm). Therefore, Zn

addition is effective to achieve dense and highly conductive specimens at a sintering temperature of 1200 °C.

3.6. The effect of Si

The Si impurity forms an intergranular phase easily[51] and promotes sintering of various oxides.[52] The increase of density at 1200 °C (Fig. 3) and significant increase of phase purity at 1200 and 1300 °C (Fig. 5) can be attributed to the liquid phase sintering and the enhanced mass transfer through the siliceous intergranular phase, respectively. The ρ_{tot} values were decreased slightly by the addition of Si (Fig. 8), mainly due to the decrease of ${\rho_{gb}}^{app}$. The addition of siliceous impurity, even at trace concentration, is known to decrease the grain-boundary conduction of acceptor-doped zirconia and acceptor-doped ceria up to several hundred times.[53–56] The highly resistive grain boundary can be mainly attributed to the formation of resistive intergranular phase. By contrast, the ${\rho_{gb}}^{app}$ values of the LSGM-Si specimens in the present study were slightly smaller than those of the LSGM specimens. In the previous contribution, the present authors[57] reported that the grain-boundary conduction of LSGM sintered at 1400 °C was hardly affected even by the addition of 500–2000 ppm of SiO_2 impurities. This was attributed to the gathering of the acidic siliceous phase near the more basic SrO component among the two basic components in LSGM: SrO and MgO. This is feasible considering a series of studies reporting that the grain-boundary conduction of GDC containing SiO_2 impurity can be greatly enhanced by the addition of alkali earth oxides such as MgO,[58] CaO,[59] SrO,[60] and BaO.[61] In the present study, the slight decrease in the ${\rho_{gb}}^{app}$ values in the LSGM-Si specimens was partially attributed to the decrease of grain-boundary density induced by the grain growth, while the lack of deterioration on the grain-boundary conduction is explained by the gathering of siliceous phase near the SrO components.

3.7. The effect of Mn, Fe, Co, Ni, and Cu

Transition metals such as Mn, Fe, Co, Ni, and Cu enhanced both the densification and phase purity (Figs. 3 and 5), except for the slight decrease of phase purity induced by Mn and Co doping at 1200 °C (Fig. 5(a)). The ρ_{tot} values of the transition-metal-doped specimens were also smaller than those of the undoped LSGM specimens except for LSGM-Ni-1200 (Fig. 8). Ishihara et al.[31] reported that the conductivity of LSGM was increased by doping with 10 at% of Co and Fe, but decreased by the doping with 10 at% of Mn and Cu. They also reported that Co- and Fe-doped specimens exhibited a conductivity that was almost independent of Po_2 from 1 to 10^{-20} atm. In contrast, substantial n- and p-type behaviors were found in reducing and oxidizing atmospheres, respectively, in the specimens doped with Mn (n-type), Ni (n-type), and Cu (p-type). This indicates that the doping with Fe and Co is effective in increasing the ionic conductivity without significant deterioration of the ionic transport number. Indeed, the ionic transport numbers of the undoped and 5 at% Co-doped LSGM specimens at ~650 °C were reported to be ~0.98 and ~0.92, respectively.[33] This is further supported by the accomplishment of high power density in SOFCs using Co- and Fe-doped LSGM.[38] In the present study, the decrease in the transport number was thought to be small considering small doping concentration (1 at%). Thus, the addition of 1 at% Co and Fe can enhance the density, phase purity, and electrical conductivity without significantly deteriorating the ionic transport number.

3.8. The effect of V

The densities and phase purity of LSGM-V-1200 and LSGM-V-1300 were significantly larger than those of LSGM-1200 and LSGM-1300, respectively (Figs. 3 and 5). Moreover, the ρ_{tot} values were also greatly decreased by the addition of V. This combination of properties reveals V as the most advantageous among all the additives. The melting point of V_2O_5 is 690 °C. It is considered one of the representative sintering additives to promote densification via liquid phase sintering.[62–65] The densification and phase purity of the V-doped LSGM specimen can therefore be attributed to the liquid phase sintering and enhanced mass transfer via intergranular liquid phase, respectively. The ρ_{gi} values decreased from 50.46 to 33.03 kΩ cm at 1200 °C and from 36.96 to 24.56 kΩ cm at 1300 °C. Thus, the possibility of V incorporation into the LSGM lattice cannot be excluded. To elucidate the role of V as a sintering additive, we are systematically studying the lattice parameters, densities, and electrical conductivities as a function of V content and sintering temperature. The results of these detailed analyses will be published later.

3.9. The effect of Li

The densities of the Li-doped LSGM specimens were the second highest (Fig. 3). By contrast, the phase purity (Fig. 5) and ρ_{gi} values (Fig. 8) were not varied significantly by the addition of Li. Thus, we considered that Li promotes the sintering of LSGM by the formation of Li-containing liquid phase.

3.10. The effects of Ba, Bi, Ca, Al

The addition of Ba deteriorated the densification (Fig. 3), phase purity (Fig. 5), and electrical conductivity (Fig. 8). The addition of Bi promoted densification at 1200 °C (Fig. 3(a)) and increased phase purity slightly at 1300 °C (Fig. 5(b)). However, the ρ_{tot} values were the highest among the specimens (Figs. 7(f) and 8). This increase of resistivity emanated not from the change in ρ_{gi} but from that in ${\rho_{gb}}^{app}$. This indicates that Bi is not incorporated into the LSGM lattice but forms a resistive intergranular phase during sintering. The addition of Ca increased the density at 1200 °C (Fig. 3(a)), phase purity at 1300 °C (Fig. 5(b)), and electrical conductivity at 1200 and 1300 °C (Fig. 8). The Al addition deteriorated the densification (Fig. 3) but slightly increased the phase purity and electrical conductivity (Figs. 5 and 8).

3.11. Specific grain-boundary resistivity

The ${\rho_{gb}}^{app}$ values in Section 3.3 were calculated from the specimen thickness (l). For more accurate analysis, the spe-

cific grain-boundary resistivity ($\rho_{gb}{}^{sp}$) should be attained from the grain-boundary thickness (δ_{gb}). Although it is difficult to estimate the precise dimension of the resistive grain-boundary phases, including the intergranular phase and oxygen vacancy depletion layer, the $\rho_{gb}{}^{sp}$ values can be calculated from the ratio of the capacitances of the grain interior and grain boundary using the following assumptions: (1) a brick layer model, (2) $\rho_{gb}{}^{sp} \gg \rho_{gi}$, (3) grain size $\gg\delta_{gb}$, and (4) permittivity of grain-boundary phase (ε_{gb}) $\cong$ permittivity of grain-interior phase (ε_{gi}).[66]

$$\rho_{gb}^{sp} = \frac{C_2}{C_1}\rho_{gb}^{app} \quad (2)$$

where C_1 and C_2 are the capacitances of the grain-interior and grain-boundary components attained by the deconvolution of the impedance spectra, respectively.

Fig. 8(c) shows the results. The $\rho_{gb}{}^{sp}$ values ranged from 4901 to 33,005 kΩ cm which were 86–246 times higher than the $\rho_{gb}{}^{app}$ values and 158–885 times higher than the ρ_{gi} values. This indicates that the grain boundaries of the LSGM specimens were several hundred times more resistive than the grain interior. The relative magnitude of the $\rho_{gb}{}^{sp}$ values was similar to that of the $\rho_{gb}{}^{app}$ values (Fig. 8(b) and (c)). The $\rho_{gb}{}^{sp}$ value of LSGM-Si-1300 was ~1.3 times more resistive than that of LSGM-1300. This can be attributed to the effect of residual siliceous intergranular phase that remained after gathering around the basic SrO-rich phase. However, compared to the several hundred fold increase in grain-boundary resistivity induced by the siliceous impurity in acceptor-doped ceria,[53–56] the Si-induced deterioration of the grain-boundary conduction in the LSGM specimen can be regarded as negligible. The grain-boundary conduction was greatly enhanced by the addition of V, Fe, Al, Co, Ni, and Zn, but significantly deteriorated by doping with Bi, B, Li, and Si.

3.12. The optimum additives

To summarize the findings of the present study, the improved densification, phase purity, and electrical conductivity of LSGM gained by doping with V, Si, Zn, Fe, and Co oxides support the promising potential of these additives. In particular, the addition of V generated the most promising results. Further research should focus on the effects of the above oxide additives on the electronic conduction, interface stability at the LSGM electrolyte, and operational stability of SOFCs.

4. Conclusion

The low-temperature sintering, phase purity, and electrical conductivity of LSGM could be controlled by the careful design of sintering aids. The densification was enhanced by the addition of V, Li and Cu, the phase purity by the addition of B, V, and Si, and the electrical conductivity by the addition of V, Fe, Zn and Cu. The variations of density, phase purity, grain-interior resistivity, and grain-boundary resistivity of the specimens were discussed in relation to the liquid-phase assisted sintering, the enhanced mass transfer, the incorporation of additives into the LSGM lattice, and the formation of resistive intergranular liquid phases, respectively. Considering all these properties, the low-temperature sintering of phase-pure and highly conductive LSGM was achieved by the addition of V, Si, Zn, Fe and Co. In particular, V showed the greatest improvement in densification, phase purity, and electrical conductivity.

Acknowledgements

This work was supported by the Korea Science and Engineering Foundation (KOSEF) NRL program grant funded by the Korean government (MEST) (no. R0A-2008-000-20032-0) and by New & Renewable Energy R&D program (20093020030040) under the Korea Ministry of Knowledge Economy (MKE).

References

1. Ishihara T. Doped $LaGaO_3$ perovskite-type oxide as a new oxide ionic conductor. *J Am Chem Soc* 1994;**116**:3801–3.
2. Feng M, Goodenough JB. Improved oxide electrolytes. *Eur J Solid State Inorg Chem* 1994;**T31**:663–72.
3. Guo W, Liu J, Zhang Y. Electrical and stability performance of anode-supported solid oxide fuel cells with strontium- and magnesium-doped lanthanum gallate thin electrolyte. *Electrochim Acta* 2008;**53**:4420–7.
4. Bozza F, Polini R, Traversa E. High performance anode-supported intermediate temperature solid oxide fuel cells (IT-SOFCs) with $La_{0.8}Sr_{0.2}Ga_{0.8}Mg_{0.2}O_{3-\delta}$ electrolyte films prepared by electrophoretic method. *Electrochem Comm* 2009;**11**:1680–3.
5. Lo C-H, Tsai C-H, Hwang C. Plasma-sprayed YSZ/Ni-LSGM-LSCo intermediate-temperature solid oxide fuel cells. *Int J Appl Ceram Technol* 2009;**6**:513–24.
6. He T, He Q, Pei L, Ji Y, Liu J. Doped lanthanum gallate film solid oxide fuel cells fabricated on a Ni/YSZ support. *J Am Ceram Soc* 2006;**89**:2664–7.
7. Majewski P, Maldener T. Synthesis and characterization of Sr- and Mg-doped $LaGaO_3$ tapes. *Int J Appl Ceram Technol* 2009;**6**:249–56.
8. Datta P, Majewski P, Aldinger F. Synthesis and microstructural characterization of Sr- and Mg-substituted $LaGaO_3$ solid electrolyte. *Mater Chem Phys* 2007;**102**:240–4.
9. Polini R, Pamio A, Traversa E. Effect of synthetic route on sintering behaviour, phase purity and conductivity of Sr- and Mg-doped $LaGaO_3$ perovskites. *J Eur Ceram Soc* 2004;**24**:1365–70.
10. Li S, Bergman B. Doping effect on secondary phases, microstructure and electrical conductivities of $LaGaO_3$ based perovskites. *J Eur Ceram Soc* 2009;**29**:1139–46.
11. Huang P, Horky A, Petric A. Interfacial reaction between nickel oxide and lanthanum gallate during sintering and its effect on conductivity. *J Am Ceram Soc* 1999;**82**:2402–6.
12. Zhu X, Suna K, Lea S, Zhang N, Fu Q, Chen X, et al. Improved electrochemical performance of NiO–$La_{0.45}Ce_{0.55}O_{2-\delta}$ composite anodes for IT-SOFC through the introduction of a $La_{0.45}Ce_{0.55}O_{2-\delta}$ interlayer. *Electrochim Acta* 2008;**54**:862–7.
13. Kim KN, Kim BK, Son JW, Kim J, Lee H-W, Lee J-H, et al. Characterization of the electrode and electrolyte interfaces of LSGM-based SOFCs. *Solid State Ionics* 2006;**177**:2155–8.
14. Huang K, Goodenough JB. A solid oxide fuel cell based on Sr- and Mg-doped $LaGaO_3$ electrolyte: the role of a rare-earth oxide buffer. *J Alloys Compd* 2000;**303–304**:454–64.
15. Huang K, Tichy RS, Goodenough JB, Milliken C. Superior perovskite oxide-ion conductor; strontium- and magnesium-doped $LaGaO_3$: III. Performance tests of single ceramic fuel cells. *J Am Ceram Soc* 1998;**81**:2581–5.

16. Cho P-S, Park S-Y, Cho YH, Kim S-J, Kang YC, Mori T, et al. Preparation of LSGM powders for low temperature sintering. *Solid State Ionics* 2009;**180**:788–91.
17. Chae NS, Park KS, Yoon YS, Yoo IS, Kim JS, Yoon HH. Sr- and Mg-doped $LaGaO_3$ powder synthesis by carbonate coprecipitation. *Colloids Surf A: Physicochem Eng Aspects* 2008;**313–314**:154–7.
18. Lee D, Han J-H, Chun Y, Song R-H, Shin DR. Preparation and characterization of strontium and magnesium doped lanthanum gallates as the electrolyte for IT-SOFC. *J Power Sources* 2007;**166**:35–40.
19. Shi M, Liu N, Xu Y, Yuan Y, Majewski P, Aldinger F. Synthesis and characterization of Sr- and Mg-doped $LaGaO_3$ by using glycine-nitrate combustion method. *J Alloys Compd* 2006;**425**:348–52.
20. Oncel C, Ozkaya B, Gulgin MA. X-ray single phase LSGM at 1350 °C. *J Eur Ceram Soc* 2007;**27**:599–604.
21. Chen T-Y, Fung K-Z. Synthesis of and densification of oxygen-conducting $La_{0.8}Sr_{0.2}Ga_{0.8}Mg_{0.2}O_{2.8}$ nano powder prepared from a low temperature hydrothermal urea precipitation process. *J Eur Ceram Soc* 2008;**28**: 803–10.
22. Jung DS, Koo HY, Jang HC, Kim JH, Cho YH, Lee J-H, et al. Firing characteristics of $La_{0.8}Sr_{0.2}Ga_{0.8}Mg_{0.2}O_{3-\delta}$ electrolyte powders prepared by spray pyrolysis. *J Alloys Compd* 2009;**487**:693–7.
23. Gonçalves P, Figueiredo FM. Mechanosynthesis of $La_{1-x}Sr_xGa_{1-y}Mg_yO_{3-\delta}$ materials. *Solid State Ionics* 2008;**179**:991–8.
24. Ishikawa H, Enoki M, Ishihara T, Akiyama T. Self-propagating high-temperature synthesis of $La(Sr)Ga(Mg)O_{3-\delta}$ for electrolyte of solid oxide fuel cells. *J Alloys Compd* 2007;**430**:246–51.
25. Liu B, Zhang Y. $La_{0.9}Sr_{0.1}Ga_{0.8}Mg_{0.2}O_{3-\delta}$ sintered by spark plasma sintering (SPS) for intermediate temperature SOFC electrolyte. *J Alloys Compd* 2008;**458**:383–9.
26. Maglia F, Anselmi-Tamburini U, Chiodelli G, Çamurlu HE, Dapiaggi M, Munir ZA. Electrical, structural, and microstructural characterization of nanometric $La_{0.9}Sr_{0.1}Ga_{0.8}Mg_{0.2}O_{3-\delta}$ (LSGM) prepared by high-pressure spark plasma sintering. *Solid State Ionics* 2009;**180**:36–40.
27. Chang J, Lee H-W, Kang S-JL. Low-temperature pressureless sintering of Sr- and Mg-doped lanthanium gallate ceramics by sintering atmosphere control. *J Am Ceram Soc* 2009;**92**:927–30.
28. Kesapragada SV, Bhaduri SB, Bhaduri S, Singh P. Densification of LSGM electrolytes using activated microwave sintering. *J Power Sources* 2003;**124**:499–504.
29. Subasri R, Mathews T, Sreedharan OM. Microwave assisted synthesis and sintering of $La_{0.8}Sr_{0.2}Ga_{0.83}Mg_{0.17}O_{2.815}$. *Mater Lett* 2003;**57**:1792–7.
30. Ohnuki M, Fujimoto K, Ito S. Preparation of high-density $La_{0.90}Sr_{0.10}Ga_{1-y}Mg_yO_{3-\delta}$ ($y = 0.30$ and 0.30) oxide ionic conductors using HIP. *Solid State Ionics* 2006;**177**:1729–32.
31. Ishihara T, Akbay T, Furutani H, Takita Y. Improved oxide ion conductivity of Co doped $La_{0.8}Sr_{0.2}Ga_{0.8}Mg_{0.2}O_3$ perovskite type oxide. *Solid State Ionics* 1998;**113–115**:585–91.
32. Trofimenko N, Ullmann H. Transition metal doped lanthanum gallates. *Solid State Ionics* 1999;**118**:215–27.
33. Ishihara T, Furutani H, Honda M, Yamada T, Shibayama T, Akbay T, et al. Improved oxide ionic conductivity in $La_{0.8}Sr_{0.2}Ga_{0.8}Mg_{0.2}O_3$ by doping Co. *Chem Mater* 1999;**11**:2081–8.
34. Trofimenko N, Ullmann H. Co-doped LSGM: composition-structure-conductivity relations. *Solid State Ionics* 1999;**124**:263–70.
35. Stenvenson JW, Hasinska K, Canfield NL, Armstrong TR. Influence of cobalt and iron additions on the electrical and thermal properties of (La, Sr)(Ga, Mg)$O_{3-\delta}$. *J Electrochem Soc* 2000;**147**:3213–8.
36. Khorkounov BA, Näfe H, Aldinger F. Relationship between the ionic and electronic partial conductivities of co-doped LSGM ceramics from oxygen partial pressure dependence of the total conductivity. *J Solid State Electrochem* 2006;**10**:479–87.
37. Enoki M, Yan J, Matsumoto H, Ishihara T. High oxide ionic conductivity in Fe and Mg doped $LaGaO_3$ as the electrolyte of solid oxide fuel cells. *Solid State Ionics* 2006;**177**:2053–7.
38. Ishihara T, Shibayama T, Honda M, Nishiguchi H, Takita Y. Intermediate temperature solid oxide fuel cells using $LaGaO_3$ electrolyte: II. Improvement of oxide ion conductivity and power density by doping Fe for Ga site of $LaGaO_3$. *J Electrochem Soc* 2000;**147**:1332–7.
39. Yoo JS, Lee S, Yu JH, Woo SK, Park H, Kim HG. Fe doping effects on phase stability and conductivity of $La_{0.75}Sr_{0.25}Ga_{0.8}Mg_yO_{0.2}$. *J Power Sources* 2009;**193**:593–7.
40. Kim HT, Kim SH, Nahm S, Byun JD, Kim Y. Low-temperature sintering and microwave dielectric properties of zinc metatitanate-rutile mixtures using boron. *J Am Ceram Soc* 1999;**82**:3043–8.
41. Wang S-F, Chung C-C, Wang C-H. Effects of B_2O_3 on the phase formation of $Ba_2Ti_9O_{20}$ ceramic. *Mater Chem Phys* 2003;**79**:256–60.
42. Wang S-F, Chung C-C, Wang C-H, Chu JP. Effects of B_2O_3 on the phase stability of $Ba_2Ti_9O_{20}$ microwave ceramic. *J Am Ceram Soc* 2002;**85**:1619–21.
43. Yuksel B, Kirtay S, Ozkan TO, Acikalin E, Erkalfa H. The effect of B_2O_3 addition to the microstructure and magnetic properties of $Ni_{0.4}Zn_{0.6}Fe_2O_4$ ferrite. *J Magnetism Magnetic Mater* 2008;**320**:714–8.
44. Han KR, Jang J-W, Cho S-Y, Jeong D-Y, Hong K-S. Preparation and dielectric properties of low-temperature-sinterable $(Zr_{0.8}Sn_{0.2})TiO_3$ powder. *J Am Ceram Soc* 1998;**81**:1209–14.
45. Huang C-L, Hou JL, Pan C-L, Huang C-Y, Peng C-W, Wei C-H, et al. Effect of ZnO additive on sintering behavior and microwave dielectric properties of $0.95MgTiO_3$–$0.05CaTiO_3$ ceramics. *J Alloys Compd* 2008;**450**:359–63.
46. Caballero AC, Fernandez JF, Moure C, Duran P, Chiang Y–M. Grain growth control and dopant distribution in ZnO-doped $BaTiO_3$. *J Am Ceram Soc* 1998;**81**:939–44.
47. Zuo R, Rödel J, Chen R, Li L. Sintering and electrical properties of lead-free $Na_{0.5}K_{0.5}NbO_3$. *J Am Ceram Soc* 2006;**89**:2010–5.
48. Tao S, Irvine JTS. A stable, easily sintered proton-conducting oxide electrolyte for moderate-temperature fuel cells and electrolyzers. *Adv Mater* 2006;**18**:1581–4.
49. Tao S, Irvine JTS. Conductivity studies of dense yttrium-doped $BaZrO_3$ sintered at 1325 °C. *J Solid State Chem* 2007;**180**:3493–503.
50. Babilo P, Haile SM. Enhanced sintering of yttrium-doped barium zirconate by addition of ZnO. *J Am Ceram Soc* 2005;**88**:2362–8.
51. Luo J. Stabilization of nanoscale quasi-liquid interfacial films in inorganic materials: a review and critical assessment. *Critical Rev Solid State Mater Sci* 2007;**32**:67–100.
52. Moon JH, Jang HM, You BD. Densification behaviors and piezoelectric properties of MnO_2, SiO_2-doped $Pb(Ni_{1/3}Nb_{2/3})O_3$–$PbTiO_3$–$PbZrO_3$ ceramics. *J Mater Res* 1993;**8**:3184–91.
53. Lee J-H. Highly resistive intergranular phases in solid electrolytes: an overview. *Monatsh Chem* 2009;**140**:1081–94.
54. Guo X, Waser R. Electrical properties of the grain boundaries of oxygen ion conductors: acceptor-doped zirconia and ceria. *Progress Mater Sci* 2006;**51**:151–210.
55. Lee J-H, Mori T, Li J-G, Ikegami T, Komatsu M, Haneda H. Improvement of grain-boundary conductivity of 8 mol% yttria-stabilized zirconia by precursor scavenging of siliceous phase. *J Electrochem Soc* 2000;**147**:2822–9.
56. Lee J-H, Mori T, Li J-G, Ikegami T, Drennan J, Kim D-Y. Precursor scavenging of resistive grain-boundary phase in 8 mol% yttria-stabilized zirconia: the effect of trace concentrations of SiO_2. *J Mater Res* 2001;**16**:2377–83.
57. Cho YH, Ha S-B, Jung D-S, Kang YC, Lee J-H. SiO_2-tolerant grain-boundary conduction in Sr- and Mg-doped lanthanum gallate. *Electrochem Solid State Lett* 2010;**13**:B28–31.
58. Cho YH, Cho P-S, Auchterlonie G, Kim DK, Lee J-H, Kim D-Y, et al. Enhancement of grain-boundary conduction in gadolinia-doped ceria by the scavenging of highly resistive siliceous phase. *Acta Mater* 2007;**55**:4807–15.
59. Cho P-S, Lee SB, Cho YH, Kim D-Y, Park H-M, Lee J-H. Effect of CaO concentration on the enhancement of grain-boundary conduction in gadolinia-doped ceria. *J Power Sources* 2008;**183**:518–23.
60. Cho P-S, Cho YH, Park S-Y, Lee SB, Kim D-Y, Park H-M, et al. Grain-boundary conduction in gadolinia-doped ceria: the effect of SrO addition. *J Electrochem Soc* 2009;**156**:B339–44.
61. Park S-Y, Cho P-S, Lee SB, Park H-M, Lee J-H. Improvement of grain-boundary conduction in SiO_2-doped GDC by BaO addition. *J Electrochem Soc* 2009;**156**:B891–6.
62. Yee KA, Han KR, Kim HT. The effect of V_2O_5 on the sinterability and physical properties of Bi_2O_3–NiO–Nb_2O_5 and

Bi_2O_3–ZnO–Nb_2O_5 temperature-stable dielectrics. *J Mater Sci* 1999;**34**: 4699–705.

63. Huang C-L, Chen Y-B, Tasi C-F. Influence of V_2O_5 additions to $0.8(Mg_{0.95}Zn_{0.05})TiO_3$–$0.2Ca_{0.61}Nd_{0.26}TiO_3$ ceramics on sintering behavior and microwave dielectric properties. *J Alloys Compd* 2008;**454**:454–9.
64. Chien Y-C, Hsu C-H, Chen K-C. Dielectric properties of $La(Mg_{0.5}Sn_{0.5})O_3$ ceramics doped with V_2O_5 at macrowave frequencies. *Ferroelectrics* 2009;**393**:54–62.
65. Yao Z, Liu H, Shen Z, Chen Z, Wu Z, Yu H, et al. Effect of V_2O_5 additive to $0.4SrTiO_3$–$0.6La(Mg_{0.5}Ti_{0.5})O_3$ ceramics on sintering behavior and microwave dielectric properties. *Mater Res Bull* 2006;**41**: 1972–8.
66. Haile SM, West DL, Campbell J. The role of microstructure and processing on the proton conducting properties of gadolinium-doped barium cerate. *J Mater Res* 1998;**13**:1576–95.